Differentiating toxic and non-toxic tri-cresyl phosphate isomers using ion-molecule reactions with oxygen

Roshanak Amiri[1], Meera J. Bissram[1], Mahin Hashemihedeshi[1], Frank L. Dorman[2,3], David Megson[4], Karl J. Jobst[1,*]

[1]*Department of Chemistry, Memorial University of Newfoundland and Labrador, St. John's, NL, Canada A1C5S7*
[2]*Department of Chemistry, Dartmouth College, Hanover, New Hampshire 03755, United State*
[3]*Waters Corporation, Milford, Massachusetts 01757, United State*
[4]*Department of Natural Science, Ecology and Environment Research Center, Manchester Metropolitan University, Manchester, UK*

Abstract: Ortho-*substituted* isomers of tricresyl phosphates (TCPs) and their toxic metabolites (e.g., CBDP: cresyl saligenin phosphate) can cause neurotoxic effects in humans. When TCP is introduced to an atmospheric pressure chemical ionization (APCI) source using gas chromatography (GC), radical cations $M^{\bullet+}$ are formed by charge exchange. The mass spectrum of an ortho-substituted isomer displays two intense peaks that are absent in the spectra of non-ortho-substituted isomers, leading us to propose structure-diagnostic ion-molecule reactions between ions $M^{\bullet+}$ and oxygen species present in the source. However, the mechanism of these reactions has not yet been established. In this study, we propose a mechanism and provide support through computational and experimental analysis using density functional theory (DFT) and cyclic ion mobility-mass spectrometry (cIM-MS). The mechanism consists of a multi-step reaction starting with the rearrangement of the molecular ion into a distonic isomer followed by an oxidation step and then, decomposition into $[CBDP\text{-}H]^+$. This proposal is consistent with the results obtained from a series of isotopically-labelled analogues. Cyclic ion mobility experiments with a triorthocresyl phosphate standard, reveals the presence of at least two hydrogen shift isomers of the product ion $[CBDP\text{-}H]^+$ that are connected by a low-lying barrier. The selectivity of the ion-molecule reactions towards ortho-substituted cresyl TCP isomers provides us with an identification tool that can select potentially neurotoxic tri-aryl phosphate esters present in complex mixtures that are produced in large volume by industry.

*Corresponding author: kjobst@mun.ca

1. Introduction

Organophosphate esters (OPEs) have been used extensively as plasticizers, lubricant additives, anti-foaming agents and substitutes for banned halogenated flame retardants. [1–3] They have been identified in air and (indoor) dust particulate, water, soil, sediment, and biota. [2–6] Among aryl OPEs, triorthocresyl phosphate (ToCP) is infamous for its neurotoxicity. [7–9] The first observations of the neurotoxic effects of ToCP in humans involved contamination of foodstuffs, beverages, and drugs, resulting in pain, paresthesia, muscle weakness and paralysis. [10] More recent studies on human exposure to ToCP have focused on aircraft crews reporting headaches, loss of balance, numbness, and neurobehavioral abnormalities as the symptoms of so-called "aerotoxic syndrome". [11,12] It has been suggested that aerotoxic syndrome is associated with the presence of ToCP in the lubricants used in jet engines. [13]

Tricresyl phosphates (TCP) with ortho-cresyl substituents exhibit greater neurotoxicity than their non-ortho counterparts. [14,15] This is because ortho-TCPs are biotransformed into toxic metabolites that cannot be generated from non-ortho substituted TCPs. For example, ToCP is metabolized to CBDP (cresyl saligenin phosphate (2-(ortho-cresyl)-4H-1,2,3-benzodioxaphosphorin-2- oxide)) by liver microsomal cytochrome P450 and serum albumin, see Scheme 1. CBDP is responsible for the neurotoxic effects of ToCP as it can irreversibly bind to human butyrylcholinesterase (hBuChE) and human acetylcholinesterase (hAChE). [16–18] Ortho substituted TCPs are also more reactive under ambient conditions, possibly because they undergo atmospheric oxidation. [5,13] Consequently, the lifetime and probability of exposure of a TCP isomer depends on the number of ortho substituents. This may explain why longer lived mono-*o*-cresyl isomers and di-*o*-cresyl isomers respectively appear to be ten- and five-fold more toxic than ToCP. [5,19]

Differentiating between TCP isomers requires efficient separation. Commonly employed methods for identifying TCP in environmental samples involve gas or liquid chromatography-mass spectrometry (LC-MS or GC-MS). [20–24] Commercially produced OPEs are mixtures that likely contain hundreds of compounds, [25] few of which are available as authentic standards.

In a previous study by Megson et al., the occurrence of TCPs and their alkylated homologues in fresh and used jet oil was investigated by comprehensive two-dimensional gas

chromatography (GCxGC) coupled with atmospheric pressure chemical ionization (APCI) mass spectrometry (GC×GC-APCI). They observed that the APCI mass spectrum of ToCP displayed two additional peaks compared to those of trimeta- and triparacresyl phosphate. [26] Although a mechanism was not proposed, the authors suggest that ion-molecule reactions with oxygen may be selective towards ortho-substituted isomers. [27–30] Ion molecule reactions involving oxygen have been shown to differentiate isomeric ions in both positive [29] and negative ion modes. [27,28,30] In the present study, we employ density functional theory to elucidate the mechanism of these ion-molecule reactions in combination with complementary experiments on D-labeled ortho-substituted TCP isomers. This study aims to establish the mechanism of the ion-molecule reactions with oxygen (in both O_2 and O_3 forms) that is selective towards the ortho-substituted TCP isomers, leading to an approach to identify toxic, ortho-substituted isomers and congeners of TCP present in environmental samples.

2. Experimental Section

2.1. Chemicals and Sample preparation: Triortho, trimeta and triparasubstituted-cresyl phosphates (ToCP, TmCP, and TpCP) were obtained from TCI America. Tris 2-ethyl phenyl phosphate and D-labeled TCP isomers (Tri-CD_3-orthocresyl phosphate, mono-D_7-meta-diorthocresyl phosphate, mono-D_7-ortho-dimetacresyl phosphate, mono-D_7-para-diorthocresyl phosphate, mono-D_7-ortho-diparacresyl phosphate, di-D_7-meta-monoorthocresyl phosphate, di-D_7-ortho-monometacresyl phosphate, di-D_7-para-monoorthocresyl phosphate, and di-D_7-ortho-monoparacresyl phosphate; Table S3) were synthesized from phosphorous (V) oxychloride (Fisher Scientific) and the corresponding alcohols (*o*-, *m*- and *p*-cresols, TCI America; D_8-labelled *o*-, *m*- and *p*-cresol, CDN Isotopes; CD_3-labelled *o*-cresol, Toronto Research Chemicals; 2-ethylphenol, TCI America) using a method adapted from Huang *et al.*, 2017 [31]. Following Huang *et al.*'s procedure, the seven syntheses performed herein produced yields ranging from 50 to 75%. The identity of each synthetic product was confirmed initially by comparing the chromatographic behaviour with that of their unlabeled analogue. The deviations between theoretical and experimental m/z were within 5 ppm for all compounds.

2.2. Instrumental Analysis: The experiments were performed using a Waters Select Series Cyclic IMS ion mobility mass spectrometer (Wilmslow, UK) coupled to an Agilent 8890 Gas chromatograph using atmospheric pressure chemical ionization (APCI). Analyte separation was

performed using either a Rtx-5HT column (15m×250µm×0.25µm) or a DB-XLB column was applied (15m×250µm×0.1µm). Most experiments were performed using an initial oven temperature set to 90 °C for 1 minute; then ramped to 115 °C at 95 °C/min, to 150 °C at 65 °C/min, to 210 °C at 45 °C/min, and to 330 °C at 35 °C/min, and finally held for 3.5 minutes with a total run time of 10 minutes. [32] For selected GC experiments, the oven temperature was ramped to 325 °C at 27 °C/min and held for 6.3 minutes with a total run time of 16 minutes. Standard solutions (1 µL) were injected in the splitless mode. The inlet temperature was set to 280 °C and the helium carrier gas flow was set to 3 mL/min. GC eluent exiting the column was swept through the ion volume using a make-up flow of nitrogen (~99.99% purity) of 350 mL/min. Atmospheric pressure chemical ionization was performed under solvent free conditions by corona discharge (2 µA) in the positive mode. Analyte molecules were ionized by charge exchange with $N_2^{\bullet+}$. The purity of the in-house nitrogen (99.99%) was too high to observe ion molecule reactions observed by Megson *et al.* [26] who employed a nitrogen generator yielding <99.5% purity. In the present study, we used dried compressed air as the auxiliary and cone gas to promote reactions with dioxygen. The source conditions were as follows: source temperature, 150 °C; sampling cone, 40 V; cone gas, 175 L/hour; auxiliary gas, 100 L/hour. Column bleed ($C_9H_{27}O_5Si_5^+$ - m/z 355.0699) was used to internally correct the measured m/z. Mass spectra were collected for m/z 50 – 1200. The cyclic ion mobility cell was operated in the single pass mode, with a separation time set to 10.64 ms and a traveling wave height of 15 V. Calibration of the instrument to measure CCS was performed according to standard procedure using a mixture of 22 compounds (aka, "major mix") supplied by Waters Corp. Multi-pass experiments were performed by increasing the separation time to 98.04 ms (8 passes) and 207.06 ms (16 passes). Collision-induced dissociation (CID) experiments were performed with nitrogen (collision energy (trap), 6 V; (transfer), 4 V) in the trap and transfer regions of the cIMS, which are located before and after the cyclic ion mobility cell, respectively.

2.3. Computational methods: All computations were performed with the Gaussian g16 suite of programs on the Atlantic Computational Excellence network (ACEnet) cluster. The total energies of all ions and neutrals were calculated using the B3LYP level of theory in combination with the 6-311G (2d,d,p) basis set. [33] The identity of local minima and connecting transition states (TS) was determined by frequency analysis and confirmed by intrinsic reaction coordinate (IRC) calculations. The total energies (in Hartree) and relative energies (in kcal/mol) for the molecular ions, product ions and neutrals are reported in Table S1, S2. The predicted collision cross section

(CCS) values of all structures were calculated using the MobCal-MPI v1.2, on ***the*** SHARCNET platform. Geometry optimization prior to MobCal analysis was performed by DFT at the B3LYP/6-31++G(d,p) level of theory. Using the python module provided by Hopkins *et al.*, [34] in combination with Open Babel 2.4.1 [35] and sdf2xyz2sdf [36] packages, the output files from the geometry optimization were converted to input files for MobCal-MPI. The trajectory method (TM) was employed to simulate CCS measurements using N_2 as the buffer gas. [34]

3. Results and Discussion

3.1. Parallels between the metabolism of ToCP and its ion-molecule reactions with oxygen. Scheme 1 displays the two-step metabolism of ToCP. First, the cresyl methyl group is oxidized into an alcohol by the microsomal enzyme cytochrome P450. The next step involves ring-closure between the newly-formed hydroxyl group and the phosphate moiety. This process is catalyzed by serum albumin, and results in the formation of CBDP, a neurotoxic metabolite. Meta- and para-substituted isomers cannot undergo the same reaction, and consequently they are less toxic. Megson *et al.* [26] observed that the APCI mass spectrum of ToCP is characterized by two additional peaks absent in those of trimeta and triparacresyl phosphate. [26]

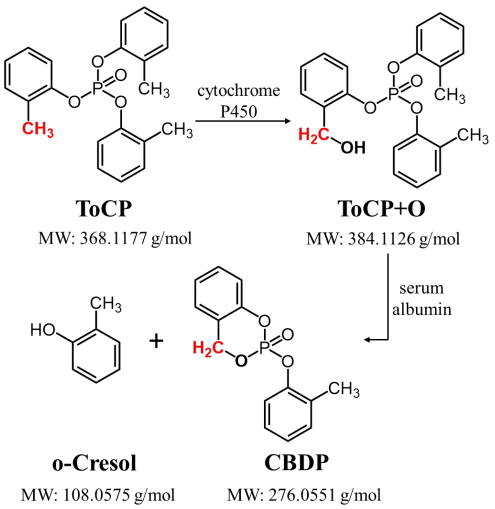

Scheme 1. The metabolism of ToCP (tri-ortho cresyl phosphate) into the toxic metabolite CBPD. [37]

Figure 1a displays the APCI (+) mass spectrum of ToCP. Compared to the mass spectra of TmCP and TpCP (Figs. S16 and S17), the spectrum of ToCP display two additional mass peaks (m/z 383 and m/z 275) in Figure 1a, are only one mass unit less than those expected for the

metabolites shown in Scheme 1. These peaks are observed when oxygen is present in the ion source, [30] (Figs. 1, and S6-17) and disappear when pure (>99.99%) nitrogen (Figure S18-30) is used as the cone and auxiliary gas. The selected ion chromatograms of isomers ToCP, TmCP and TpCP in Figure 2 indicate that only ToCP can produce m/z 275 product ions. The exact mass measured for m/z 275 deviates 1.1 ppm from the theoretical mass of $C_{14}H_{12}PO_4$, which contains one less hydrogen atom than the elemental composition of CBDP. The mass spectrum of ToCP (Figure 1a) also displays a negligible yield of molecular ions $M^{\bullet+}$ compared to those of TmCP and TpCP (Figs. S7/S8), which suggests that almost all molecular ***radical cations (***$M^{\bullet+}$***)*** of ToCP have reacted with oxygen species present in the source. This is also reflected in the selected ion chromatograms of ions $M^{\bullet+}$ (m/z 368) and $[M+H]^+$ (m/z 369) shown in Figures 2a/b: the ***abundances*** of the $[M+H]^+$ ions of all three isomers (ToCP, TmCP and TpCP) are approximately equal, whereas the $M^{\bullet+}$ ions resulting from ToCP are depleted. These results suggest that oxygen reacts with the $M^{\bullet+}$ ions, whereas the $[M+H]^+$ quasimolecular ions probably do not play a significant role in the reaction.

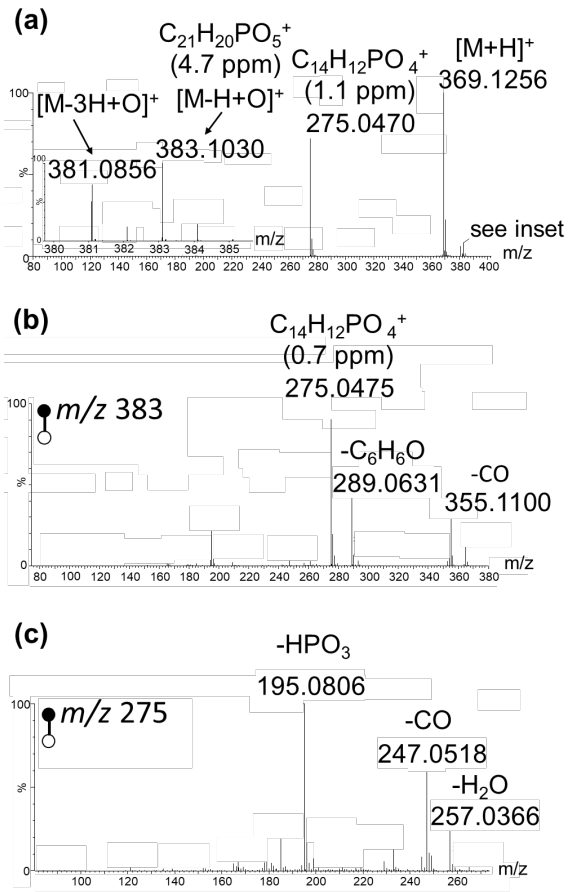

Figure 1. (a) APCI$^+$ mass spectrum of ToCP (ToCP$^{\bullet+}$ radical cation [m/z 368.1177] was not observed); CID mass spectra of **(b)** m/z 383 and **(c)** m/z 275 ions generated from ToCP. Note: The m/z 275 region of the mass spectrum in **(a)** is magnified by 10-fold.

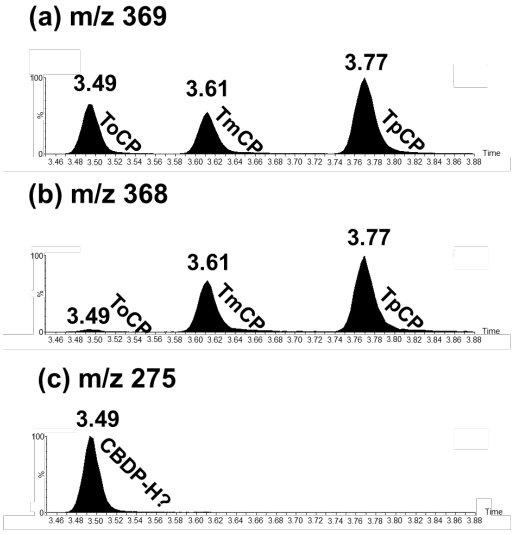

Figure 2. Selected ion chromatograms of **(a)** $[M+H]^+$ (m/z 369); **(b)** $M^{\bullet+}$ (m/z 368); and **(c)** $[CBDP-H]^+$ m/z 275 ions generated by an equimolar mixture of ToCP, TmCP and TpCP.

The m/z 383 product shown in Figure 1a (inset) deviates by 4.7 ppm from the theoretical mass of $C_{21}H_{20}PO_5$, which contains one less hydrogen atom than the metabolite generated in the first step of the metabolic process in Scheme 1. If the m/z 383 ions are intermediates in the ion-molecule reactions, then one would expect that the CID mass spectrum of m/z 383 would display an intense peak corresponding to ions with m/z 275. The observation from CID experiments (Figure 1b) is consistent with the proposal that ToCP radical cations react with oxygen to form m/z 383 ions $[M-H+O]^+$, which subsequently dissociate into $[CBDP-H]^+$ as the final product of the ion-molecule reactions. Unfortunately, the mass spectrum of the m/z 275 ion (see Figure 1c) is dominated by reactions (losses of H_2O, CO and HPO_3) that are not helpful in elucidating its structure.

At first glance, the ion-molecule reactions observed in Figure 1a parallel the metabolic process shown in Scheme 1. [38] In both, activation of a C-H bond at the ortho-methyl moiety is a key step. However, human metabolism of ToCP achieves C-H bond activation through enzyme catalysis, whereas the ion-molecule reactions appear to be uncatalyzed. Ayrton *et al.* [38] have observed that uncatalyzed oxidation of saturated hydrocarbons can occur in an ambient corona

discharge, under similar conditions to those used in our experiments, and leading to $[M-H+O]^+$ ions among other oxidation products. They argue that ozone is likely responsible for these oxidation processes, and this proposal is based on the observation that saturated hydrocarbons typically form abundant $[M-H]^+$ ions, which can readily react with ozone. We suspect that the mechanism of the ion-molecule reactions involving ToCP are different for three reasons. First, $[M-H]^+$ ions were not observed in the mass spectra of ToCP or its isomers, and it isn't immediately obvious why ozonation of the ortho-methyl group would be favoured over the meta- or para-isomers. Secondly, we observed depletion of the molecular ions $M^{\bullet+}$ of ToCP, which strongly suggests that the radical cation is the likely reactant. Third, organophosphate ester ions are likely to form long-lived, stable distonic ions [39] that may be reactive towards both molecular oxygen [29] and ozone.

3.2. Computational analysis of the mechanism. Figure 3 displays the energy diagram of the proposed mechanism for the ion-molecule reactions involving O_2. The first step involves rearrangement of ion **TCP1** into its distonic isomer **TCP2** via a 1,6-H shift. The molecular ion must have at least 18 kcal/mol of internal energy to overcome the initial energy barrier. Upon charge exchange with $N_2^{\bullet+}$ (~15 eV), incipient $TCP^{\bullet+}$ ions will have 7 eV (~161 kcal/mol) of internal energy. However, most of the initial internal energy will be removed by collisional cooling. Stephens et al. [40] used a set of thermometer ions with well-defined dissociation energies to study the distribution of internal energies resulting from APCI. Their results suggest that the average internal energy of $TCP^{\bullet+}$ ions is approximately 30-40 kcal/mol, [40] which exceeds the 18 kcal/mol barrier required for transformation of TCP1 into TCP2. The radical site of the distonic isomer (**TCP2**) offers an attractive site for triplet O_2 to form a covalent bond. [29] This results in the generation of the remarkably stable ion **TCP3a**. The newly formed C-O bond is stabilized by at least 19 kcal/mol. Consequently, ion **TCP3a** can rearrange by low lying hydrogen shifts into **TCP4a** and **TCP5a**.

The next stage of the reaction involves the loss of $^{\bullet}OH$ from **TCP5a** via a direct bond cleavage, which would explain the formation of $[M-H+O]^+$ ions, as witnessed by the m/z 383 peak in Figure 1a. This reaction is predicted to be exothermic: the dissociation threshold (**TCP6** + $^{\bullet}OH$) lies 41 kcal/mol below the combined enthalpies of the reactants **TCP1** and O_2. However, our calculations also suggest that the loss of $^{\bullet}OH$ is associated with a substantial kinetic barrier. To

probe the transition state structure, we performed a relaxed scan of the potential energy surface along the peroxyl bond. At each step of the calculation, the O-O bond was increased stepwise, while the remaining parts of the ion were allowed to optimize. Instead of a smooth direct bond cleavage reaction into **TCP6** + ˙OH, we found that this led to rearrangement of **TCP5a** into a ter-body complex, **TBC1**, shown in Scheme 2.

The terbody complex **TBC1** consists of three discrete species, bound together non-covalently: a dicresyl phosphite radical cation complexed with a cresyl radical and a hydroxyl radical. Dissociation of ions **TBC1** by loss of a cresyl radical requires only 9 kcal/mol and the loss of a cresol molecule requires only 3 kcal/mol. It is important to note that cresyl radical loss, resulting in m/z 293 ions, is not observed experimentally. Therefore, we suggest that further rearrangement of ions **TBC1** must occur via pathways that do not exceed the energy requirements for loss of a cresyl radical. The calculations indicate that the least energy demanding route to loss of ˙OH from ions **TBC1**, see Scheme 2, involves migration of the cresyl radical in **TBC1** towards the dicresyl phosphite moeity, resulting in the formation of a phosphorous-oxygen bond. Unfortunately, the barrier for this reaction exceeds the energy requirements for cresyl radical loss, a reaction that is not observed.

From the computed mechanism shown in Fig. 3, we conclude that the reaction between **TCP1** and O_2 can produce the observed m/z 383 ions, either from **TCP5a** via a direct bond cleavage, or via a rearrangement into the ter-body complex **TBC1**. However, the presence of a kinetic barrier seems to impede the formation of m/z 383 ions by this route, and the absence of m/z 293 in the mass spectrum (Fig. 1a) also casts doubt on this mechanism. One possible explanation is that the reaction does not involve dioxygen, but rather other oxygen species present in the source, such as ozone.

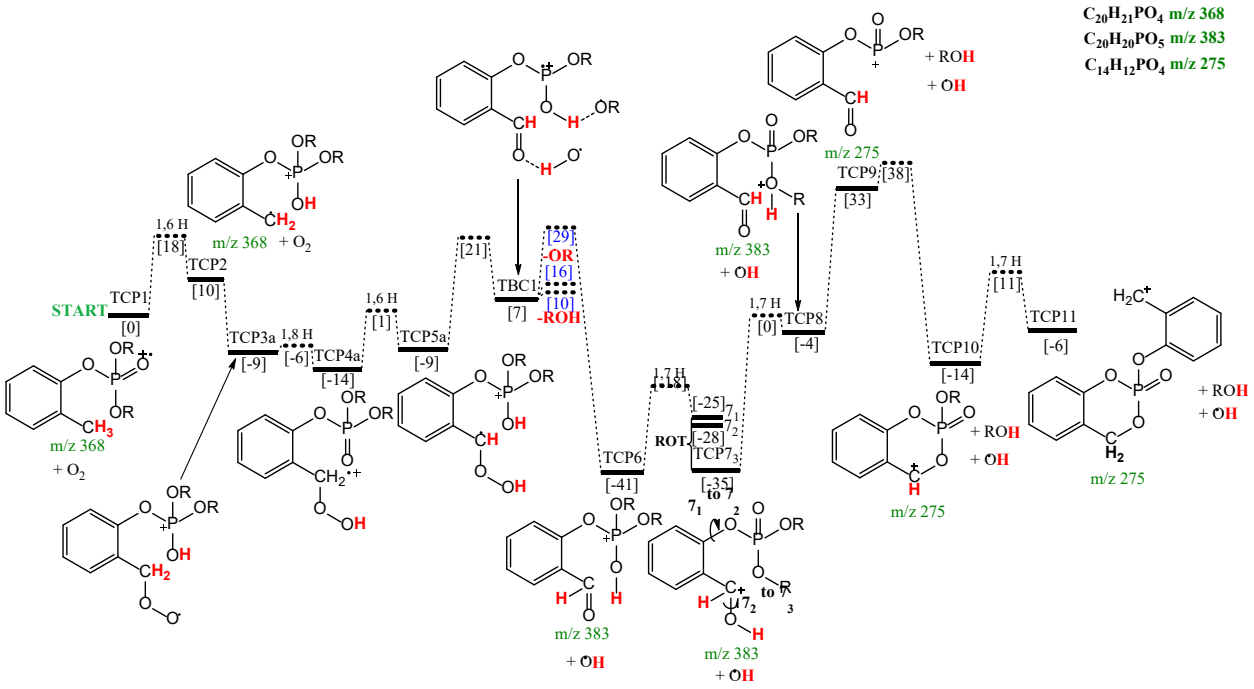

Figure 3. Energy diagram depicting the proposed mechanism for the ion-molecule reactions of ToCP$^{\bullet+}$ with O_2. The numbers in square brackets are relative energies (in kcal/mol) from **Table S1**. Note: R represents the o-cresyl group.

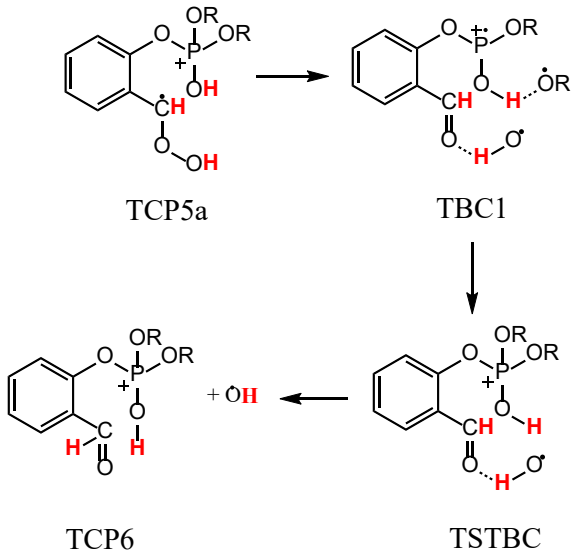

Scheme 2. Rearrangement of TCP5a to TBC1 and TSBC, resulting in the formation of TCP6+ $^{\bullet}$OH.

Figure 4 displays the proposed ion-molecule reactions mechanism involving ozone. Most steps of this mechanism parallel those proposed in the reaction with O_2. The first step involves rearrangement of the molecular ion **TCP1** into its distonic isomer **TCP2**. Then, O_3 reacts with **TCP2**, by forming a strong C-O bond in ion **TCP3b** that is stabilized by 80 kcal/mol. Ion **TCP3b**

can follow two possible paths to produce **TCP6** by loss of a peroxyl radical (˙OOH), resulting in the observed m/z 383 ions.

TCP3b could rearrange into **TCP6** via a circuitous route involving consecutive 1,9 H- and 1,6-H shifts (not shown), but the least energy demanding pathway involves a straightforward 1,4-H shift. Ion **TCP6** can then rearrange into **TCP8** via a 1,7 H-shifts and then decompose by loss of a cresol molecule to form m/z 275 ions **TCP9.** We note that **TCP9** can also ring-close into a more stable isomer, **TCP10**, which is closely similar in structure to CBDP. Overall, the formation of m/z 383 and m/z 275 from **TCP1** and ozone is highly exothermic: The CBDP analogue **TCP10** is generated with upwards of 88 kcal/mol of internal energy! Thus, **TCP10** can easily isomerize into **TCP11** via a low-lying 1,7-H shift, and we would therefore expect that the m/z 275 ions consist of a mixture of at least two or more H-shift isomers. This hypothesis will be tested by ion mobility experiments described in **Section 3.4**. In the proposed mechanism, the hydrogens on the ortho methyl groups (shown in red in Figure 3) play a crucial role. **Section 3.3** explores the use of isotopically labeled analogues to support the proposed mechanism.

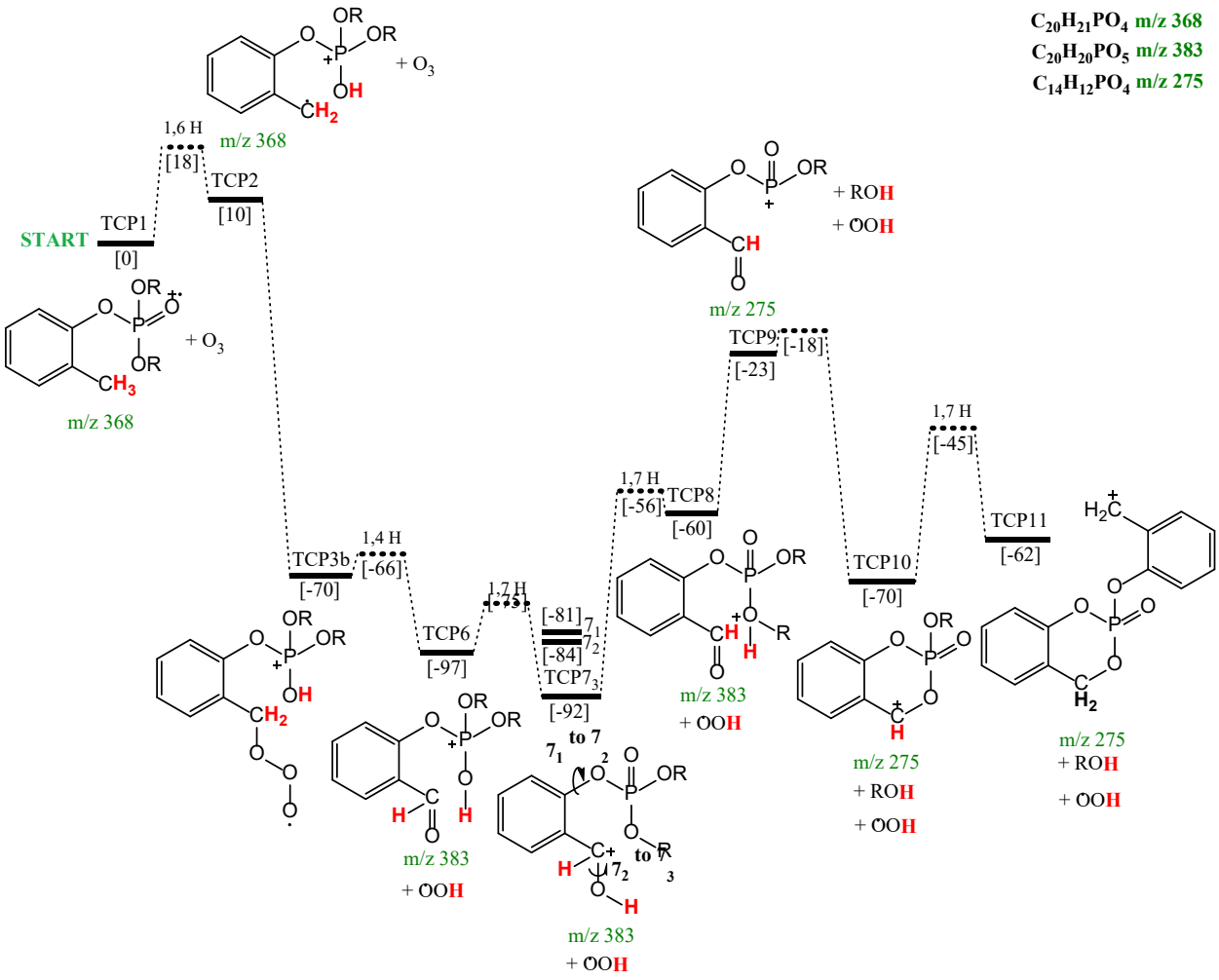

Figure 4. Energy diagram depicting the proposed mechanism for the ion-molecule reactions of ToCP$^{\bullet+}$ with O_3. The numbers in square brackets are relative energies (in kcal/mol) from **Table S2**. Note: Each R represents the o-cresyl group.

3.3. Complementary experiments with (isotopically labeled) isomers and homologues. Isotopic labeling in mass spectrometry is a time-honored approach to study the mechanisms of ion-molecule reactions and dissociations.[41] This section describes experiments with the D-labeled ToCP analogues and isomers listed in Table S3 and S4. The proposed mechanism (Figure 4) suggests that the ortho-methyl hydrogen atoms play a crucial role in the reaction. Therefore, one would expect that experiments with CD_3-labeled ToCP would result in mass shifted products compared to the reaction with unlabeled ToCP. Indeed, the APCI mass spectrum of CD_3-labeled ToCP, see Figure 5, displays peaks at m/z 390, corresponding to the loss of $^{\bullet}$OD from the incipient

ion molecule complex **TCP3b**, and m/z 279 which corresponds with the $[CBDP\text{-}D]^+$ ions. These observations are consistent with the mechanistic proposal shown in Figure 4.

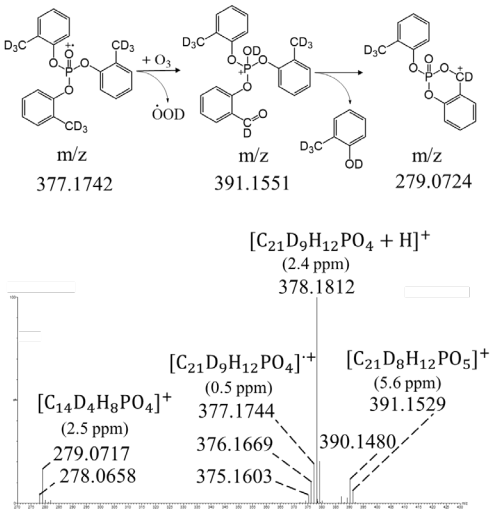

Figure 5. The $APCI^+$ mass spectrum of D_9-labeled (methyl CD_3) triorthocresyl phosphate (tri-CD_3-*o* CP).

Compared to its unlabeled analogue, the mass spectrum of CD_3-labelled ToCP also displays two additional peaks that appear at one and two mass units less than the molecular ion mass (m/z 377 and m/z 376) as well as the $[M\text{-}D+O]^+$ and $[CBDP\text{-}D]^+$ product ions masses (m/z 390 and m/z 278), see Figure 5. Accurate mass measurements suggest that the additional peaks could result from hydrogen-deuterium exchange between the ion structures and water molecules present in the ion source. The mechanism for this exchange has not been investigated, but we note that the distonic ion **TCP2** contains a phosphoryl hydrogen (or deuterium in the case of the CD_3-labeled analogue) that could potentially be exchanged. The mass spectra of the synthesized D_7- and D_{14}- labelled TCPs provide support for this proposal by revealing that only TCPs that are labelled on the ortho-substituted cresyl group(s) form H-D exchange products, see Figures S9, S11, S13 and S15. When oxygen is excluded from the source, the putative exchange reactions mostly disappear, which suggests that the exchange may involve intermediates generated during the ion-molecule reactions.

Among the remaining eight synthesized D-labelled ortho-substituted tricresyl phosphates, three of them (mono-D_7-ortho-dimeta CP, mono-D_7-para-diortho CP, and di-D_7-ortho-monometa CP) formed all expected $[M\text{-}H/D+O]^+$ and $[CBDP\text{-}H/D]^+$ product ions (Table S4). For example, di-D_7-ortho-monometa CP is expected to react with ozone to produce [CBDP-D]+ ions while

losing either a mass-labelled ortho cresol molecule or an unlabeled meta cresol molecule. In this case, both reactions are observed (see Fig. S14). The mass spectra of four other labelled compounds (mono-D_7-meta-diortho CP, di-D_7-ortho-monopara CP, di-D_7-meta-monoortho CP, and di-D_7-para-monoortho CP) display mass peaks corresponding to $[M\text{-}H/D+O]^+$ product ions, but only one or none of the expected $[CBDP\text{-}H/D]^+$ product ions. In all these cases, the cresol expected to be lost was D_7-labelled, which suggests a kinetic isotope effect impedes the formation of $[CBDP\text{-}H/D]^+$ ions. Finally, the last synthesized isotopologue, mono-D_7-ortho-dipara CP, did *not* lose *p*-cresol-OD, which is only labelled with one deuterium. We note that *p*-cresol is the least stable cresol isomer by ~2 kcal/mol[42], thus increasing the dissociation threshold. The loss of cresol-OD also requires a deuterium shift that may be impeded by a kinetic isotope effect. The ethyl-substituted ToCP homologue, tri-*o*-ethyl phenylphosphate (ToEP) was studied to test the hypothesis that the reaction involving ToCP will also occur in its homologues that contain at least one ortho-methylene. In the mass spectrum obtained in the presence of oxygen, peaks corresponding to both $[M\text{-}H+O]^+$ and $[M\text{-}H+O\text{-}ROH]^+$ ions (m/z 425 and m/z 303) were observed.

3.4. Characterization of the $[CBDP\text{-}H]^+$ product ions using ion mobility. The mechanism proposed in Figure 4 indicates that the m/z 275 product ions are generated as a mixture of hydrogen shift (H-shift) isomers, viz. **TCP9**, **TCP10** and **TCP11**. Theory predicts that the least stable isomer, **TCP9**, swiftly rearranges via a low barrier into ions **TCP10** and **TCP11**. Therefore, it is expected that the population of *m/z* 275 ions primarily consists of two isomers, **TCP10** and **TCP11**, which may be separable by ion mobility. This hypothesis was tested by the ion mobility experiments shown in Figure 6, which display retention time vs. drift time contour plots of the m/z 275 ions generated by ToCP. When the m/z 275 ions generated in the ion source are subjected to one pass through the cyclic ion mobility cell, three mobility separated peaks are resolved (Fig. 6a), of which two will be shown to be genuine m/z 275 isomers, while one is an artefact.

Three peaks are observed in the contour plot of Figure 6a with drift times of ~23, 24.5 and 29 ms. We propose that the peak observed at a drift time of 29 ms is the result of metastable dissociation of m/z 383 ions into m/z 275 ions after exiting the cIMS cell. Indeed, when the collision energy is increased in the transfer region located downstream of the cIMS cell, the abundance of the m/z 275 peak observed with a drift time of 29 ms dramatically increases (Fig.

7c) whereas the abundances of the two peaks at 23 and 24.5 ms increase when collision-induced dissociation occurs prior to the cIMS cell (Fig. 7b). The collision cross section of the ions observed with a drift time of 23 ms was measured to be 149.6 $Å^2$, which deviates by -4.1% from the value computed for **TCP10** using MobCal-MPI. Theory also predicts that the separation of **TCP10** and **TCP11** requires a resolving power of 45 (defined as R=CCS/ΔCCS), which is line with the expected performance of the instrument when ions are subjected to a single pass through the cIMS cell.

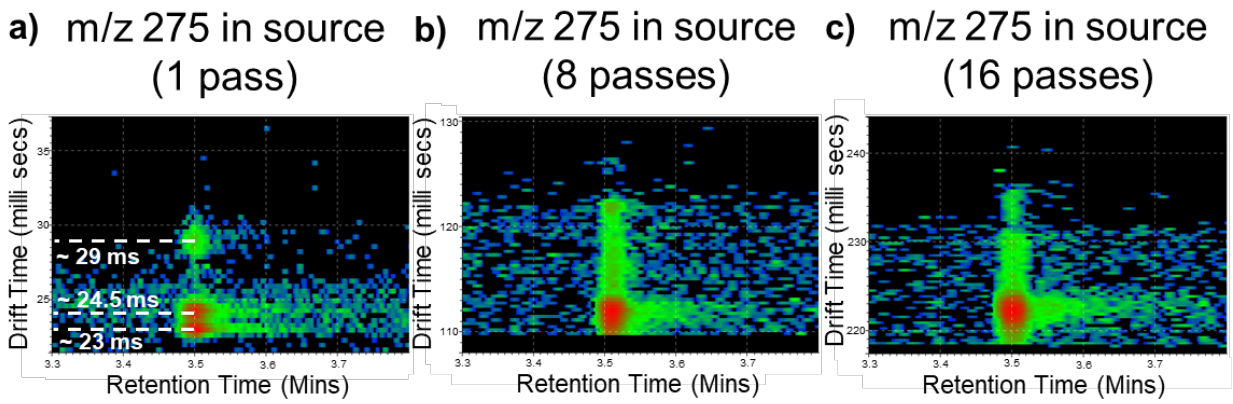

Figure 6. Selected ion contour plots of m/z 275 ions that have travelled (a) 1 pass; (b) 8 passes; and (c) 16 passes through the cIMS cell. The two peaks at ~23 ms and ~24.5 ms correspond to genuine m/z 275 isomers separated by ion ***mobility***. The peak at ~29 ms is an artefact peak resulting from metastable decomposition of m/z 383 ions occurring downstream of the cIMS cell. The BGR color scale was used to display intensity.

In principle, the separation of ions **TCP10** and **TCP11** could be improved by allowing the ions to travel successive passes through the cIMS cell. However, when the number of passes is increased to eight (Fig. 6b) and sixteen (Fig. 6c), the separation does not improve, and the two peaks instead coalesce. This experimental observation is in agreement with theory, which predicts that ions **TCP10** and **TCP11** are connected by a transition state that lies 45 kcal/mol below the initial energy of the molecular ion, see Fig. 4. When multi-pass experiments are performed, each additional pass provides ions TCP10 and TCP11 with more time to interconvert during their transit through the cIMS cell. We also considered the possibility that ions **TCP10** and **TCP11** rearrange by ring-expansion into ions **TCP12** and **TCP13**, whose structures are shown in Figure S31. Ions

TCP12 and **TCP13** are the products of benzylium-tropylium rearrangement. However, the energy barriers of these rearrangements are estimated to be as high as 50 kcal/mol based on the previous study by Zins *et al.* [43].

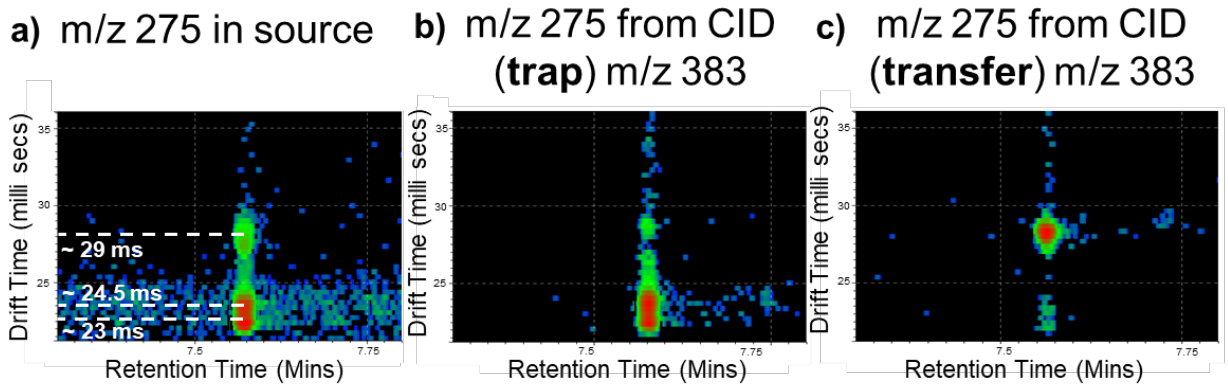

Figure 7. Selected ion contour plots of m/z 275 ions (a) generated in the source; and generated from mass selected m/z 383 ions that undergo CID in trap (b) and transfer (c) collision cells.

4. Conclusions

The neurotoxic congeners of TCP undergo a two-step metabolism, involving oxidation into M+O followed by decomposition into the metabolite CBDP. This biochemical process parallels the proposed mechanism for the ion-molecule reactions between ionized ToCP with oxygen species present in the APCI source. Computational analysis of the ion-molecule reactions indicates that the reaction between ionized ToCP and O_3 is less energy demanding than the reaction involving O_2. Experimental support for the selectivity of the reaction toward the ortho-cresyl group(s) was provided by performing mass spectrometry analysis on deuterium labelled ortho-substituted TCP isomers. The results also suggest that a distonic ion plays a crucial role in the reaction. Experiments with the ethyl-substituted ToCP homologue indicated that the ion-molecule reactions occur on ortho-substituted ethyl group(s) as well as methyl group(s). Ion-mobility separation of the products of the ion-molecule reactions revealed the formation of at least two m/z 275 isomers of $[CBDP-H]^+$. The present study provides new insight into a structure-diagnostic ion-molecule reactions that may eventually be used to identify potentially toxic congeners of homologous tri-aryl phosphates present in complex mixtures produced in large volume by industry.

5. Acknowledgements

This research was funded by the Canada Foundation for Innovation (CFI), the Natural Sciences and Engineering Research Council (NSERC), the Newfoundland and Labrador Department of Industry, Energy and Technology.

6. Supporting Information

Figure displaying optimized geometries, mass spectra of D-labelled and homologous TCP isomers. Tables summarizing the structures of D-labeled TCP isomers and computed CCS values.

References

(1) Duarte, D. J.; Rutten, J. M. M.; van den Berg, M.; Westerink, R. H. S. In Vitro Neurotoxic Hazard Characterization of Different Tricresyl Phosphate (TCP) Isomers and Mixtures. *Neurotoxicology* **2017**, *59*, 222–230. https://doi.org/10.1016/j.neuro.2016.02.001.

(2) Wei, G. L.; Li, D. Q.; Zhuo, M. N.; Liao, Y. S.; Xie, Z. Y.; Guo, T. L.; Li, J. J.; Zhang, S. Y.; Liang, Z. Q. Organophosphorus Flame Retardants and Plasticizers: Sources, Occurrence, Toxicity and Human Exposure. *Environ. Pollut.* **2015**, *196*, 29–46. https://doi.org/10.1016/j.envpol.2014.09.012.

(3) Yang, Y.; Xiao, Y.; Chang, Y.; Cui, Y.; Klobučar, G.; Li, M. Intestinal Damage, Neurotoxicity and Biochemical Responses Caused by Tris (2-Chloroethyl) Phosphate and Tricresyl Phosphate on Earthworm. *Ecotoxicol. Environ. Saf.* **2018**, *158* (April), 78–86. https://doi.org/10.1016/j.ecoenv.2018.04.012.

(4) Bollmann, U. E.; Möller, A.; Xie, Z.; Ebinghaus, R.; Einax, J. W. Occurrence and Fate of Organophosphorus Flame Retardants and Plasticizers in Coastal and Marine Surface Waters. *Water Res.* **2012**, *46* (2), 531–538. https://doi.org/10.1016/j.watres.2011.11.028.

(5) van der Veen, I.; de Boer, J. Phosphorus Flame Retardants: Properties, Production, Environmental Occurrence, Toxicity and Analysis. *Chemosphere* **2012**, *88* (10), 1119–1153. https://doi.org/10.1016/j.chemosphere.2012.03.067.

(6) He, C. T.; Zheng, J.; Qiao, L.; Chen, S. J.; Yang, J. Z.; Yuan, J. G.; Yang, Z. Y.; Mai, B. X. Occurrence of Organophosphorus Flame Retardants in Indoor Dust in Multiple Microenvironments of Southern China and Implications for Human Exposure. *Chemosphere* **2015**, *133*, 47–52. https://doi.org/10.1016/j.chemosphere.2015.03.043.

(7) Craig, P. H.; Barth, M. L. Evaluation of the Hazards of Industrial Exposure to Tricresyl Phosphate:A Review and Interpretation of the Literature. *J. Toxicol. Environ. Heal. - Part B Crit. Rev.* **1999**, *2* (4), 281–300. https://doi.org/10.1080/109374099281142.

(8) Long, D. X.; Wu, Y. J. Growth Inhibition and Induction of G1 Phase Cell Cycle Arrest in Neuroblastoma SH-SY5Y Cell by Tri-Ortho-Cresyl Phosphate. *Toxicol. Lett.* **2008**, *181* (1), 47–52. https://doi.org/10.1016/j.toxlet.2008.06.871.

(9) Li, Y.; Piao, F.; Liu, X. *Protective Effect of Taurine on Triorthocresyl Phosphate (TOCP)-Induced Cytotoxicity in C6 Glioma Cells. In Taurine 8*; Springer US, 2013.

(10) INOUE, N.; FUJISHIRO, K.; MORI, K.; MATSUOKA, M. Triorthocresyl Phosphate Poisoning. *J. UOEH* **1988**, *10* (4), 433–442. https://doi.org/10.7888/juoeh.10.433.

(11) Schopfer, L. M.; Masson, P.; Lamourette, P.; Simon, S.; Lockridge, O. Detection of Cresyl Phosphate-Modified Butyrylcholinesterase in Human Plasma for Chemical Exposure Associated with Aerotoxic Syndrome. *Anal. Biochem.* **2014**, *461*, 17–26. https://doi.org/10.1016/j.ab.2014.05.021.

(12) Liyasova, M.; Li, B.; Schopfer, L. M.; Nachon, F.; Masson, P.; Furlong, C. E.; Lockridge, O. Exposure to Tri-o-Cresyl Phosphate Detected in Jet Airplane Passengers. *Toxicol. Appl. Pharmacol.* **2011**, *256* (3), 337–347. https://doi.org/10.1016/j.taap.2011.06.016.

(13) de Ree, H.; van den Berg, M.; Brand, T.; Mulder, G. J.; Simons, R.; Veldhuijzen van Zanten, B.; Westerink, R. H. S. Health Risk Assessment of Exposure to TriCresyl Phosphates (TCPs) in Aircraft: A Commentary. *Neurotoxicology* **2014**, *45*, 209–215.

https://doi.org/10.1016/j.neuro.2014.08.011.

(14) Ramsden, J. J. On the Proportion of Ortho Isomers in the Tricresyl Phosphates Contained in Jet Oil. *J. Biol. Phys. Chem.* **2013**, *13* (2), 69–72. https://doi.org/10.4024/03ra13l.jbpc.13.02.

(15) Casida, J. E.; Eto, M.; Baron, R. L. Biological Activity of a Tri-o-Cresyl Phosphate Metabolite. *Nature* **1961**, *191*.

(16) Reinen, J.; Nematollahi, L.; Fidder, A.; Vermeulen, N. P. E.; Noort, D.; Commandeur, J. N. M. Characterization of Human Cytochrome P450s Involved in the Bioactivation of Tri-Ortho-Cresyl Phosphate (ToCP). *Chem. Res. Toxicol.* **2015**, *28* (4), 711–721. https://doi.org/10.1021/tx500490v.

(17) Carletti, E.; Colletier, J. P.; Schopfer, L. M.; Santoni, G.; Masson, P.; Lockridge, O.; Nachon, F.; Weik, M. Inhibition Pathways of the Potent Organophosphate CBDP with Cholinesterases Revealed by X-Ray Crystallographic Snapshots and Mass Spectrometry. *Chem. Res. Toxicol.* **2013**, *26* (2), 280–289. https://doi.org/10.1021/tx3004505.

(18) Masson, P. Evolution of and Perspectives on Therapeutic Approaches to Nerve Agent Poisoning. *Toxicol. Lett.* **2011**, *206* (1), 5–13. https://doi.org/10.1016/j.toxlet.2011.04.006.

(19) Dietrich Henschler. Die Trikresylphosphatvergiftung - Experimentelle Klarung von Problemen Der Atiologie Und Pathogenese. *Klin. Wochenschr.* **1958**, *36* (14), 663–674.

(20) Yang, F.; Ding, J.; Huang, W.; Xie, W.; Liu, W. Particle Size-Specific Distributions and Preliminary Exposure Assessments of Organophosphate Flame Retardants in Office Air Particulate Matter. *Environ. Sci. Technol.* **2014**, *48* (1), 63–70. https://doi.org/10.1021/es403186z.

(21) Lazarov, B.; Swinnen, R.; Spruyt, M.; Maes, F.; Van Campenhout, K.; Goelen, E.; Covaci, A.; Stranger, M. Air Sampling of Flame Retardants Based on the Use of Mixed-Bed Sorption Tubes—a Validation Study. *Environ. Sci. Pollut. Res.* **2015**, *22* (22), 18221–18229. https://doi.org/10.1007/s11356-015-5028-z.

(22) Suparanon, T.; Phetwarotai, W. Fire-Extinguishing Characteristics and Flame Retardant Mechanism of Polylactide Foams: Influence of Tricresyl Phosphate Combined with Natural Flame Retardant. *Int. J. Biol. Macromol.* **2020**, *158*, 1090–1101. https://doi.org/10.1016/j.ijbiomac.2020.04.131.

(23) Makinen, M. S. E.; Makinen, M. R. A.; Koistinen, J. T. B.; Pasanen, A. L.; Pasanen, P. O.; Kalliokoski, P. J.; Korpi, A. M. Respiratory and Dermal Exposure to Organophosphorus Flame Retardants and Tetrabromobisphenol A at Five Work Environments. *Environ. Sci. Technol.* **2009**, *43* (3), 941–947. https://doi.org/10.1021/es802593t.

(24) De Nola, G.; Kibby, J.; Mazurek, W. Determination of Ortho-Cresyl Phosphate Isomers of Tricresyl Phosphate Used in Aircraft Turbine Engine Oils by Gas Chromatography and Mass Spectrometry. *J. Chromatogr. A* **2008**, *1200* (2), 211–216. https://doi.org/10.1016/j.chroma.2008.05.035.

(25) Vykoukalová, M.; Venier, M.; Vojta, Š.; Melymuk, L.; Bečanová, J.; Romanak, K.; Prokeš, R.; Okeme, J. O.; Saini, A.; Diamond, M. L.; Klánová, J. Organophosphate Esters Flame Retardants in the Indoor Environment. *Environ. Int.* **2017**, *106* (January), 97–104. https://doi.org/10.1016/j.envint.2017.05.020.

(26) Megson, D.; Ortiz, X.; Jobst, K. J.; Reiner, E. J.; Mulder, M. F. A.; Balouet, J. Chemosphere A Comparison of Fresh and Used Aircraft Oil for the Identi Fi Cation of Toxic Substances Linked to Aerotoxic Syndrome. *Chemosphere* **2016**, *158*, 116–123. https://doi.org/10.1016/j.chemosphere.2016.05.062.

(27) Lépine, F.; Boismenu, D.; Milot, S.; Mamer, O. A. Collision of Molecular Anions of Benzenedicarboxylic Esters with Oxygen in a Triple Quadrupole Mass Spectrometer. *J. Am. Soc. Mass Spectrom.* **1999**, *10* (12), 1248–1252. https://doi.org/10.1016/S1044-0305(99)00105-1.

(28) Mamer, O. A.; Choiniere, L.; Boismenu, D.; Lepine, F. Artefactual Pyruvate and 2-Oxobutyrate Produced by Trimethylsilylation of Methylmalonic and Ethylmalonic Acids in the Presence of Oxygen. *J. Inherit. Metab. Dis.* **1999**, *22* (7), 821–826. https://doi.org/10.1023/A:1005510224963.

(29) Jobst, K. J.; De Winter, J.; Flammang, R.; Terlouw, J. K.; Gerbaux, P. Differentiation of the Pyridine Radical Cation from Its Distonic Isomers by Ion-Molecule Reactions with Dioxygen. *Int. J. Mass Spectrom.* **2009**, *286* (2–3), 83–88. https://doi.org/10.1016/j.ijms.2009.06.012.

(30) Fernando, S.; Green, M. K.; Organtini, K.; Dorman, F.; Jones, R.; Reiner, E. J.; Jobst, K. J. Differentiation of (Mixed) Halogenated Dibenzo-p-Dioxins by Negative Ion Atmospheric Pressure Chemical Ionization. *Anal. Chem.* **2016**, *88* (10), 5205–5211. https://doi.org/10.1021/acs.analchem.6b00255.

(31) Huang, X.; Zhao, X.; Zhang, M.; Xu, Y.; Zhi, H.; Yang, J. Green Synthesis of Triaryl Phosphates with POCl3 in Water. *ChemistrySelect* **2017**, *2* (34), 11007–11011. https://doi.org/10.1002/slct.201702215.

(32) Di Lorenzo, R. A.; Lobodin, V. V.; Cochran, J.; Kolic, T.; Besevic, S.; Sled, J. G.; Reiner, E. J.; Jobst, K. J. Fast Gas Chromatography-Atmospheric Pressure (Photo)Ionization Mass Spectrometry of Polybrominated Diphenylether Flame Retardants. *Anal. Chim. Acta* **2019**, *1056*, 70–78. https://doi.org/10.1016/j.aca.2019.01.007.

(33) Gaussian 16, Revision C.01, Frisch, M. J.; Trucks, G. W.; Schlegel, H. B.; Scuseria, G. E.; Robb, M. A.; Cheeseman, J. R.; Scalmani, G.; Barone, V.; Petersson, G. A.; Nakatsuji, H.; Li, X.; Caricato, M.; Marenich, A. V.; Bloino, J.; Janesko, B. G.; Gomper, W. C. Gaussian 16, Revision C.01. 2016.

(34) Ieritano, C.; Crouse, J.; Campbell, J. L.; Hopkins, W. S. A Parallelized Molecular Collision Cross Section Package with Optimized Accuracy and Efficiency. *Analyst* **2019**, *144* (5), 1660–1670. https://doi.org/10.1039/c8an02150c.

(35) O'Boyle, N. M.; Banck, M.; James, C. A.; Morley, C.; Vandermeersch, T.; Hutchison, G. R. Open Babel. *J. Cheminform.* **2011**, *3* (33), 1–14.

(36) Tosco, P.; Balle, T.; Shiri, F. SDF2XYZ2SDF: How to Exploit TINKER Power in Cheminformatics Projects. *J. Mol. Model.* **2011**, *17* (11), 3021–3023. https://doi.org/10.1007/s00894-011-1111-7.

(37) Eto, M.; Casida, J. E.; Eto, T. Hydroxylation and Cyclization Reactions Involved in the Metabolism of Tri-O-Cresyl Phosphate. *Biochem. Pharmacol.* **1962**, *11* (4–5), 337–352. https://doi.org/10.1016/0006-2952(62)90056-4.

(38) Ayrton, S. T.; Jones, R.; Douce, D. S.; Morris, M. R.; Cooks, R. G. Uncatalyzed, Regioselective Oxidation of Saturated Hydrocarbons in an Ambient Corona Discharge. *Angew. Chemie - Int. Ed.* **2018**, *57* (3), 769–773. https://doi.org/10.1002/anie.201711190.

(39) Zeller, L.; Farrell, J.; Vainiotalo, P.; Kenttämaa, H. I. Long-Lived Radical Cations of Simple Organophosphates Isomerize Spontaneously to Distonic Structures in the Gas Phase. *J. Am. Chem. Soc.* **1992**, *114* (4), 1205–1214. https://doi.org/10.1021/ja00030a013.

(40) Stephens, E. R.; Dumlao, M.; Xiao, D.; Zhang, D.; Donald, W. A. Benzylammonium Thermometer Ions: Internal Energies of Ions Formed by Low Temperature Plasma and Atmospheric Pressure Chemical Ionization. *J. Am. Soc. Mass Spectrom.* **2015**, *26* (12), 2081–2084. https://doi.org/10.1007/s13361-015-1272-1.

(41) Holmes, J. L.; Jobst, K. J.; Terlouw, J. K. Isotopic Labelling in Mass Spectrometry as a Tool for Studying Reaction Mechanisms of Ion Dissociations. *J. Label. Compd. Radiopharm.* **2007**, *50* (11–12), 1115–1123. https://doi.org/10.1002/jlcr.1386.

(42) Cox, J. D. The Heats of Combustion of Phenol and the Three Cresols. *Pure Appl. Chem.* **1961**, *2* (1–2), 125–128. https://doi.org/10.1351/pac196102010125.

(43) Zins, E. L.; Pepe, C.; Rondeau, D.; Rochut, S.; Galland, N.; Tabet, J. C. Theoretical and Experimental Study of Tropylium Formation from Substituted Benzylpyridinium Species. *J. Mass Spectrom.* **2009**, *44* (1), 12–17. https://doi.org/10.1002/jms.1461.

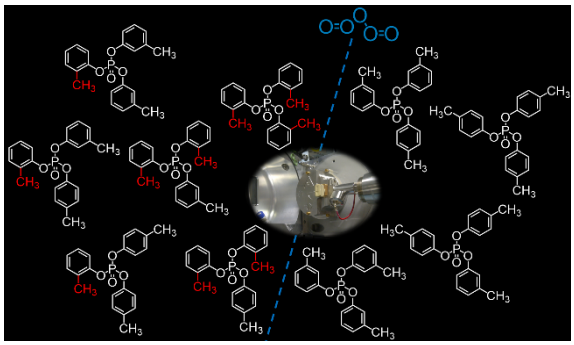

For Table of Contents Only